EULER BASED INDUCED DRAG ESTIMATION FOR HIGHLY NON-PLANAR LIFTING SYSTEMS DURING CONCEPTUAL DESIGN

J. Schirra[1], RMIT University, School of Aerospace, Mechanical & Manufacturing Engineering, Melbourne, Australia
FH Aachen University of Applied Sciences, Department of Flight Systems, Flight Guidance and Control, Aachen, Germany

J. Watmuff[2], RMIT University, School of Aerospace, Mechanical & Manufacturing Engineering, Melbourne, Australia

Abstract

Implementation of Euler based induced drag estimation is considered exemplary for two planar and two highly non-planar lifting systems employing farfield analysis technique. Basic induced drag characteristics are provided by means of farfield analysis established as well as on linear potential methodology employing a vortex-lattice approach. Euler based span efficiencies are found to agree reasonably with those predicted by potential theory, although individual spanloads and downwash distribution differ considerably. Particular for the crescent biplane, reduced downwash compensates performance penalties introduced by uneven distribution of lift. Supposed impact of higher order effects on induced drag characteristics of highly non-planar lifting systems could not be verified for systems under consideration.

NOMENCLATURE

b	=	span, *[m]*
C_D	=	Drag coefficient, *[/]*
C_L	=	Lift coefficient, *[/]*
c	=	chord, *[m]*
D	=	Drag, *[N]*
E	=	Span efficiency, *[/]*
$\vec{\imath}$	=	x-component of the unit normal vector (1, 0, 0), *[/]*
h/b	=	Height to span ratio, *[/]*
M	=	Mach number, *[/]*
$\vec{n}$	=	Unit normal vector (n_x, n_y, n_z), [/]
p	=	Pressure, *[Pa]*
R	=	Gas constant, *[J/kg·K]*
s	=	Entropy, *[J/K]*
$\vec{V}$	=	Velocity vector (u, v, w), *[m/s]*
γ	=	Specific heat ratio, *[/]*
ΔH	=	Variation of total enthalpy relative to freestream, *[J/kg]*
Δs	=	Variation of entropy relative to freestream, *[J/K]*
S	=	Surface, *[m²]*
α	=	Angle of attack, *[°]*
Λ	=	Aspect ratio, *[/]*
η	=	relative span, *[/]*
ρ	=	Density, *[kg/m³]*
Ω	=	Volume, *[m³]*

Subscript

ell	=	Elliptical
i	=	induced
ff	=	Farfield
LE	=	Leading edge
ref	=	Reference
r	=	Root
t	=	Tip
∞	=	Freestream

1. INTRODUCTION

For a commercial aircraft during stationary cruise flight, induced drag accounts for roughly 40% of the total drag. In other flight conditions its contribution can be even more profound. For take-off or landing, induced drag constitutes up to 90% having major impact on flight performance as explained by Kroo [18]. Several concepts for reducing this drag portion have been presented over the last decades. Besides rather conventional approaches like wing tip extensions (e.g. winglets), more radical concepts regain attention. Renewed interest has emerged in highly non-planar lifting systems which has led to several conceptual design studies recently. (e.g. Jemitola and Fielding [16], Salam and Bil [24], [25], Foong and Djojodihardjo [9], Jansen et al. [15], Mamla and Galinski [20], Verstraeten and Slingerland [32], Hicken and Zingg [11], Demasi [4], Sun et al. [29]). FIG 1 provides an overview of different highly non-planar lifting systems and associated theoretical span efficiencies.

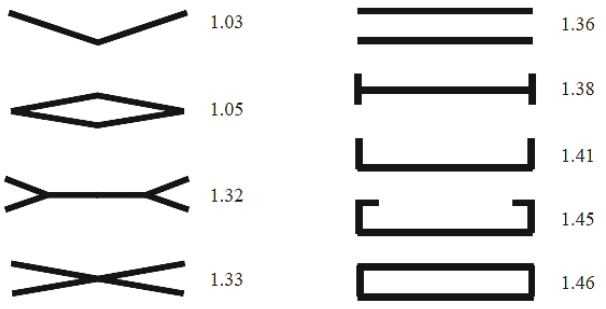

FIG 1. Highly non-planar lifting systems, Kroo [17]

Within these studies, induced drag estimates are commonly obtained by means of numerical approaches based on linear potential flow theory. Accounting for the large design

[1] Research assistant FH Aachen University of Applied Sciences, PhD student RMIT University
[2] Senior lecturer RMIT University, Senior research scientist ELORET / NASA Ames Research Center

space during conceptual design phase, the low computational effort involved makes these extremely attractive, facilitating a rapid evaluation. Vortex-lattice and panel methods are classical representatives, prescribing the trailing wake as a flat and thin vorticity sheet leaving the trailing edge in the freestream direction. Although this shape differs generally from the physical, rolled-up and force-free wake, sufficiently accurate induced drag estimates can be provided for planar wings at small angle of attack. (Smith and Kroo [28]). In particular, this is enabled by the streamlined wake model itself, only permitting force contributions perpendicular to each trailing vortex filament. The wake is therefore essentially drag free. Roll-up process can be assumed to occur so slowly that the near-field portions of the wake, having the most dominant influence on the bound vorticity and therewith on the induced drag, are not extensively altered from their initial shape.

The validity of this assumption however becomes problematic in the context of highly non-planar lifting systems. The vertical displacement of the lifting elements promotes a high degree of non-planar character in the near-wake, potentially exaggerating non-linear wing-wake interactions. By means of a hybrid wake-relaxation procedure, Smith [26] imposingly demonstrated that even for planar wings, higher order effect have a perceptible impact on the induced drag which should not be disregarded. For a split-tip planform, creating a non-planar wake, induced drag estimates obtained with streamwise and force-free wake model differed significantly (Smith [26]). Even for the well-known elliptical wing, deviations between force-free and drag-free model are evidently given.

Induced lift is another important non-linear effect, which, unlike wake shape is unique to non-planar lifting concepts. It is generated by the vertical components of the bound vorticity, in- or decreasing the local streamwise velocity and therewith altering the near-field. A wake shed by a non-planar system is therefore not necessarily lift free, conflicting with the simple farfield lift model based on drag free wake shape. The inseparable relationship between induced drag and lift makes this is a critical issue.

Computational methods based on the Euler equations depict the most comprehensive inviscid flow model and provide an improved representation of the vortical flowfield. Trailing wake shape is inherently included in the solution process and is not required to be specified a priori. Non-linear effects, systematically neglected by linear potential methods can therefore be resolved. However, induced drag prediction based on Euler equations is not compelled to provide more accurate estimates compared to linear potential methods. Part of problem certainly stems from the application of surface pressure integration (near-field approach) and cancellation of opposing pressure forces close in magnitude on inadequate dense grids (Chao and van Dam [3]). Although refining may introduce some improvement, it does not remove the source of problem completely but increases computational effort. This can be a critical point within conceptual design where a quick estimation is mandatory especially when optimization procedures are involved. Numerical diffusion, whether introduced explicitly for stability reasons or implicitly in the discretization process, distorts accurate induced drag prediction (e.g. van Dam and Nikfetrat [31], Chao and van Dam [3], Bourdin [2]).

Mid- and farfield approaches have been successfully employed to circumvent these issues. Motivated by momentum theorem, integration of flow field variables is performed on cutting planes downstream of the lifting element (Trefftz plane) or involves volume integration over parts of the computational domain. In contrast to surface pressure integration technique, mid- and farfield approaches permit drag decomposition and therewith a phenomenological breakdown into physical components.

Although mid- and farfield approaches have made their proof over years, the technique has not been integrated into any commercial CFD code yet. Very recent experience with these methods in conjunction with Navier-Stokes solver can be found in Destarac [5], Gariépy et al. [10], Hue, D. and Esquieu [13] and Vos et al. [33].

The present work intends to illustrate basic induced drag characteristics of two planar and two highly non-planar lifting systems obtained by means of a commercial Euler flow code. Comparison is made towards estimates based on linear potential methodologies using lifting line as well as biplane theory and a vortex-lattice method. Comment is given concerning the accuracy and necessity of Euler based induced drag estimation methodology with particular focus on highly non-planar lifting systems during conceptual design phase.

2. EULER BASED INDUCED DRAG ESTIMATION

2.1 Farfield drag estimation theory

This section briefly discusses the farfield drag extraction methodology presented by Destarac and van der Vooren [6]. In general, farfield approaches provide a number of advantages over nearfield methods. A critical obstacle in its application is related to the creation of spurious entropy drag due to numerical diffusion and smearing of the vortical wake on progressively coarsen grids. Induced drag decays as the location of Trefftz plane is moved downstream while spurious drag shows the opposing trend. Different approaches are available to correct farfield induced drag.

Assuming that upstream and lateral flowfield boundaries are sufficiently far away of the lifting system, the general farfield drag expression on a Trefftz plane can be given as:

$$(1) \qquad D_{ff} = \iint_{S_{TP}} \left(\rho(u-u_\infty)\left(\vec{V}\cdot\vec{n}\right) + (p-p_\infty)\vec{\imath}\right) dS$$

Fundamental idea of drag decomposition is based on the separation of the axial velocity defect into components correlating to reversible or irreversible phenomena. Since viscous and wave drag are not considered within this work, spurious entropy drag represents the only irreversible source while induced drag is related to the reversible process of adding transverse kinetic energy to the flow downstream of the lifting element exclusively. Destarac and van der Vooren [6] employed thermodynamic properties to describe the axial velocity defect due to irreversible phenomena as follows:

$$(2) \qquad \Delta\bar{u} = u_\infty \sqrt{1 + 2\frac{\Delta H}{u_\infty^2} - \frac{2}{(\gamma-1)M_\infty^2}\left[\left(e^{\frac{\Delta s}{R}}\right)^{\frac{\gamma-1}{\gamma}} - 1\right]} - u_\infty$$

Applying Gauss theorem, the drag force produced due to irreversible phenomena can be expressed as:

(3) $$D_{irreversible} = \iiint_{\Omega} \left(\nabla \cdot \rho \Delta \bar{u} \vec{V}\right) d\Omega$$

Here the volumetric integration is performed over the entire control or fluid domain Ω. Limiting the integration to areas of irreversible drag production, in the present case to the flow volume Ω_{wake} containing the trailing wake, equation (3) gives the spurious entropy drag created as:

(4) $$D_{spurious} = \iiint_{\Omega_{wake}} \left(\nabla \cdot \rho \Delta \bar{u} \vec{V}\right) d\Omega_{wake}$$

Performing estimation on a sufficient large Trefftz plane, far enough downstream for longitudinal gradients to be negligible, induced drag is given as suggested by Bourdin [2]:

(5) $$D_i = \iint_{S_{TP}} \vec{f_i} \cdot \vec{n}\, dS$$

with the vector $\vec{f_i}$

(6) $$\vec{f_i} = \frac{\rho_\infty}{2} \begin{pmatrix} v^2 + w^2 - (1 - M_\infty^2)\Delta u^{*2} \\ -2v\Delta u^* \\ -2w\Delta u^* \end{pmatrix}$$

The axial velocity defect due to reversible processes is expressed by Δu^* and can be calculated via:

(7) $$\Delta u^* = u - u_\infty + u_\infty \left(\frac{1}{\gamma M_\infty^2}\frac{\Delta s}{R} - \frac{\Delta H}{u_\infty^2}\right)$$

Direct estimation based on equation (6) leads to an underestimation of induced drag due to exchange with spurious entropy drag as Trefftz plane proceeds downstream. By applying equation (4) to a control volume bounded between vortex origin and Trefftz plane, induced drag estimates can be corrected and become independent of Trefftz plane location.

(8) $$D_{i,corrected} = D_i + D_{Spurious}$$

2.2 Euler solver

Simulation results are obtained with the commercial solver *ANSYS Fluent 14.5* [1], employing a cell-centered finite volume formulation for Euler flow equations. According to the steady and incompressible flow conditions (M_∞=0.2), the segregated pressure based solver and second order upwind spatial discretization scheme with high order term relaxation is used. Hybrid initialization is performed enabling the external-aero favourable settings. Equation (4) and (5) are implemented into *Fluent* as user-defined field function and monitored as convergence criteria. This is important since, judging convergence based on nearfield estimates is inappropriate as stated by Gariépy et al. [7]. The solution is considered to be converged when induced drag coefficients vary less than 0.1 drag count per 100 iterations.

3 PLANAR REFERENCE SYSTEMS

This section discusses relevant test cases and flow conditions for validation purpose of the presented farfield analysis within *ANSYS Fluent 14.5*. To limit the complexity, to avoid undesirable distortion by compressibility effects and to assure comparability towards results issued from other sides by means of linear potential methods, the flow is studied at a Mach number of M_∞=0.2 and an angle of attack of α=4°.

3.1 Planform geometry

Two planar systems, characterized by an elliptical chord distribution are considered.

(9) $$c(\eta) = c_r\sqrt{(1-\eta^2)}$$

In particular, these are the classical elliptical wing, having an unswept straight quarter-chord line (x_t=0.25) and a planform with an unswept straight trailing edge (x_t=1.00), referred to as crescent wing. The leading edge location is given by:

(10) $$x_{LE}(\eta) = x_t(1 - \sqrt{(1-\eta^2)})$$

Both systems are untwisted using *NACA 0012* airfoil sections with sharp trailing edge. To avoid numerical issues, the span is generally terminated close to the wing tip (η=0.999) to achieve a non-zero chord length.

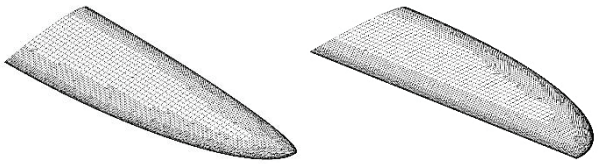

FIG 2. Isometric view elliptical and crescent planform

Elliptical and crescent planform are illustrated in FIG 2. Geometrical data describing both lifting systems can be found in TAB 1.

b [m]	b/2 [m]	η (b/2) [/]	S_{ref} [m²]	Λ [/]	c_r [m]	c_t [m]
5.491	2.745	0.999	4.318	6.982	1.000	0.051

TAB 1. Geometric properties planar reference systems

Planforms have been chosen advisedly being very well documented and validated. Foremost the crescent wing was analysed thoroughly within numerous studies (e.g. van Dam [30], Hunt et al. [14], Smith and Kroo [28], Lam and Maull [19], Mortara and Maughmer [21], Smith and Kroo [27]). Hereby, the crescent planform depicts an important special case as it achieve least induced drag of all planar systems, but also sheds planar wake at a certain angle of attack. As non-linear impact on induced drag, introduced by non-planar wake can therefore not be expected, the streamlined wake model provides exact representation within linear potential methodology. Deviations between induced drag estimation based on drag-free and force-free wake shape using Euler codes are therefore not likely to exit. This is in contrast to the elliptical wing shedding a non-planar wake and potentially exhibiting non-linear impact on induced drag. Although the amount may be admit able small, discrepancies are noticeable as pointed out by Smith [16].

3.2 Numerical grid

Grids are created using the *CutCell* Cartesian meshing approach within *ANSYS Workbench 14.5*. This type of gridding strategy is found most suitable for present purpose as it delivers high element quality while requiring minimum user input, facilitating an integration into optimization procedures during conceptual design. Rapid size changes due to hanging-node configurations can be accomplished, resulting in grids typically containing 80-95% hex cells,

yielding potentially very accurate solutions (*ANSYS* [1]). Curvature based refinement is enabled to provide sufficient element size and density in respective regions (e.g. leading edge). Explicit sizing function are employed at trailing edge and in wake region (body of influence).

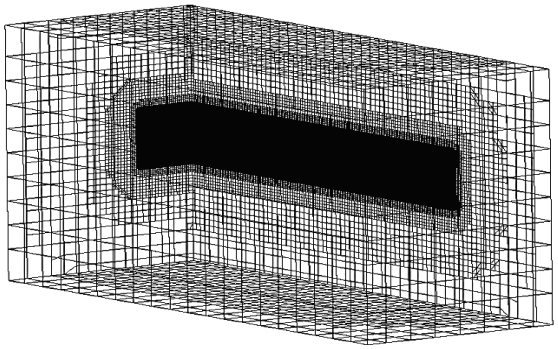

FIG 3. *CutCell* based grid

Grid sensitivity studies are performed based on a set of continuously refined grids and a Richardson extrapolation adapted from Ferziger and Peric´ [8]. The computational domain is rectangular shaped with its outer dimensions being 40x15x20 meters throughout the study. The downstream boundary is placed 27m away from the lifting system. Element numbers range from approximately 1 million to 4 million for the coarsest to finest grid respectively.

4 HIGHLY NON-PLANAR LIFTING SYSTEMS

The geometric properties of two highly non-planar lifting systems are presented in the following. Like for the planar reference systems, induced drag characteristics are studied at a Mach number of M_∞=0.2 and an angle of attack of α=4° using *ANSYS Fluent 14.5*.

4.1 Planform geometry

As shown in FIG 1, various highly non-planar systems are conceivable. For present analysis, a biplane arrangement is found most favourable, as the lifting system does not experience any planform intersections; vertical geometry components do not exist.

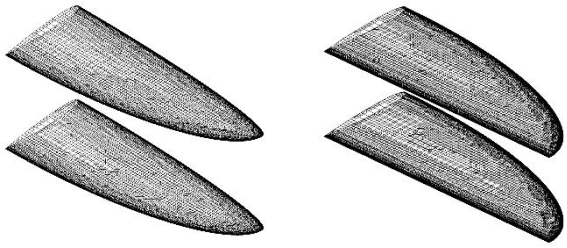

FIG 4. Isometric view elliptical and crescent biplane

This does simplify the geometry creation and gridding process to a great extent. More important, flow interactions introduced by intersecting lifting elements (e.g. X-Wing) or between horizontal and vertical lifting surfaces (e.g. C-Wing), undesirable during this early stage of analysis, are avoided. The non-linear impact by induced lift should therefore be restricted to contribution resulting from angle of attack and are not related to geometric non-planarity itself. Derived from the classical elliptical and crescent wing planform described in section 3.1, local chord distribution is given by equations (9) and (10) as well. FIG 4 shows both lifting systems, referred to elliptical and crescent biplane. Geometrical data describing both planforms can be found in TAB 2.

b [m]	b/2 [m]	η (b/2) [/]	S_{ref} [m²]	Λ [/]	c_r [m]	c_t [m]	h/b [/]
5.491	2.745	0.999	8.636		1.000	0.051	0.200

TAB 2. Geometric properties non-planar lifting systems

Equal airfoil sections (*NACA 0012*) are used; planforms do not incorporate any geometric twist. The height to span ratio (h/b) was chosen to a common value of 0.2, while no longitudinal staggering was implemented. By definition, conclusions concerning non-linear impact on Munk's stagger theorem [22] cannot be given anyway, as condition of minimum induced drag are not enforced actively and therewith not fulfilled.

4.2 Numerical grid

A set of continuously refined grids are generated for both non-planar lifting systems using Cartesian *CutCell* meshing approach. Shape of computational domain and outer dimensions comply with those presented for the planar systems under section 3.2. Element numbers range from approximately 2 million to 6 million for the coarsest to finest grid respectively.

5 RESULTS AND DISCUSSION

Results gained for planar, as well as for both highly non-planar systems are presented in the following. In the present context, span efficiency is defined as the induced drag of a system producing an ideal elliptical spanload relative to the induced drag of an arbitrary system carrying same lift at equal projected span.

$$e = \frac{C_{Di_{ell}}}{C_{Di}} \tag{11}$$

Comparison is made towards linear potential methodologies, employing lifting line theory and the vortex lattice code *AVL* [7]. Estimates within *AVL* are obtained by means of Trefftz plane analysis. The impact of panel density and spacing was studied carefully. Half-cosine spacing in spanwise direction and a cosine spacing in chordwise direction employing 60x50 elements was found to yield converged results (compare Hoefling et al [12]).

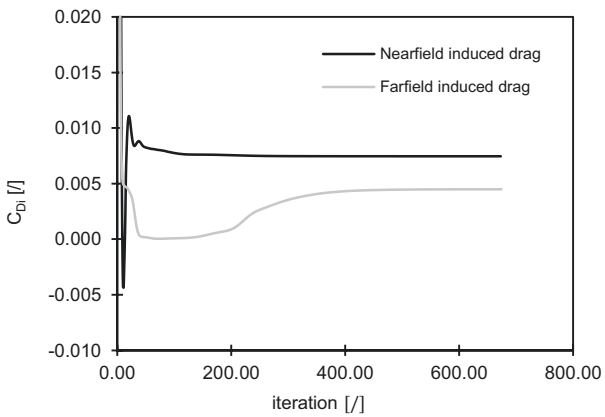

FIG 5. Convergence plot

A convergence plot is provided exemplary in FIG 5. It becomes obvious, that convergence judging based on nearfield is inappropriate for present analysis technique. To obtain converged farfield results, higher amount of iterations is mandatory.

5.1 Planar reference systems

Span efficiencies computed with *ANSYS Fluent 14.5* are given in TAB 3 based on standard surface pressure integration, as well as on the farfield technique discussed in section 2. In addition theoretical prediction based on lifting line theory and vortex-lattice methodology are provided.

Elliptical planform			
e_{LLT} [/]	e_{AVL} [/]	e_{SP} [/]	e_{FF} [/]
1.000	0.994	0.704	0.995

Crescent planform			
e_{LLT} [/]	e_{AVL} [/]	e_{SP} [/]	e_{FF} [/]
1.000	0.999	0.726	1.001

TAB 3. Planar span efficiencies

Span efficiencies obtained by means of lifting line theory equal unity for both planforms as chord is distributed elliptical. Assessing accuracy in respect to these theoretical values, Euler based surface pressure integration approach is found to differ considerably (about 30% relative), independent of planform. Although this had been expected for reasons described above, the extent of deviation is very high. In contrast to that, Euler based farfield estimation yields significantly improved results. Estimates deviate less than 1% from lifting line theory but indicate minor efficiency differences between both planforms. This trend was already reported by Smith [17], ascribing this effect to a more elliptical spanload adopted by the crescent planform. In fact, analysing corresponding spanloads for elliptical and crescent wing from the *Fluent* solution in FIG 6, Smith's finding is confirmed.

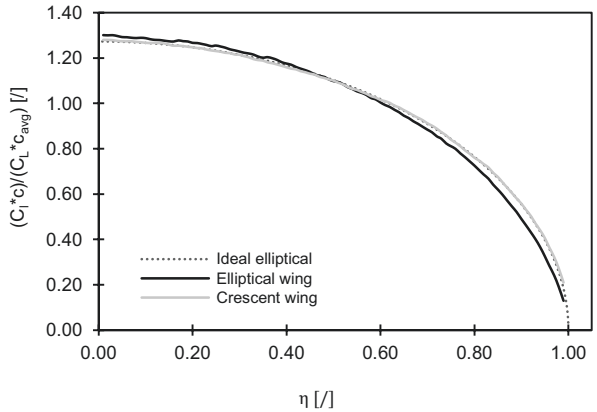

FIG 6. Spanload for elliptical and crescent wing (*Fluent*)

However, the non-linear impact on induced drag due to non-planar wake shed by elliptical planform as described by Smith [26] could not be reproduced. Its contribution is therefore assumed to negligible as estimates obtained with *AVL* agree reasonably well with Euler based farfield analysis and also emphasize potential performance benefits for crescent wing planform.

The local downwash, created by the elliptical and crescent planform are plotted against the dimensionless span coordinate in FIG 7. Downwash shed by crescent wing accords to the ideal constant pattern over large portion of its span. Although of similar magnitude, local downwash of the elliptical wing deviates from constant distribution, foremost in the tip region, delivering a further indicator for performance penalties experienced in respect to theoretical baseline and crescent planform.

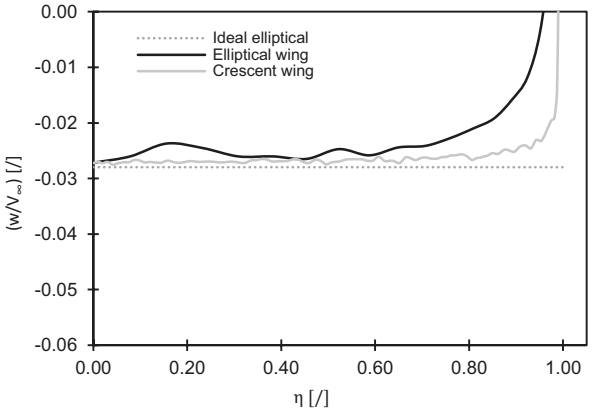

FIG 7. Downwash for elliptical and crescent wing (*Fluent*)

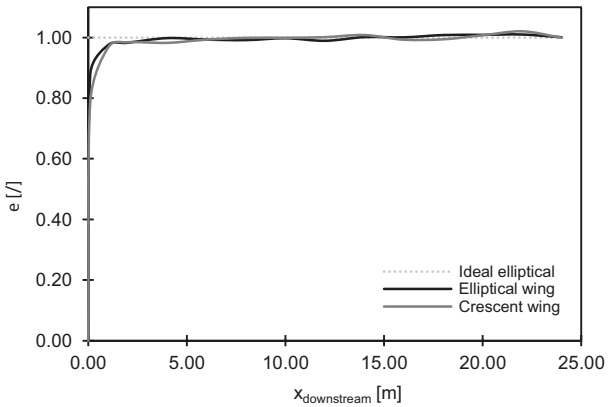

FIG 8. Span efficiency against downstream distance

Effectiveness and accuracy of presented Euler based farfield approach and correction methodology is demonstrated in FIG 8. Employing equations (2) to (8) correcting induced drag by the fraction exchanged with spurious entropy due to non-physical, irreversible phenomena, estimates become independent of downstream location. However, positioning Trefftz plane to close to the lifting system or the downstream flowfield boundary should be avoided as this can introduce numerical errors to the solution. (Gariépy et al. [7])

5.2 Highly non-planar lifting systems

TAB 4 provides span efficiencies for elliptical and crescent biplane, corresponding to estimation methodologies employed above. Subjected to the condition of evenly distributed lift, theoretical predictions based on lifting line/biplane theory are presented informally. A deliberate interpretation is however mandatory since an exact compliance of this constraint was not enforced actively within vortex-lattice and Euler based analysis. Although this

might entail a disadvantage, it prevents distortion by optimization procedure implemented to fulfil condition of minimum induced drag by modifying local twist or incidence angle.

Elliptical biplane			
e_{LLT} [/]	e_{AVL} [/]	e_{SP} [/]	e_{FF} [/]
1.360	1.348	0.961	1.342

Crescent biplane			
e_{LLT} [/]	e_{AVL} [/]	e_{SP} [/]	e_{FF} [/]
1.360	1.351	0.984	1.352

TAB 4. Highly non-planar span efficiencies

Estimates established on vortex lattice methodology show good agreement with minimum induced drag predicted by linear lifting line/biplane theory. The relative deviation in respect to theoretical baseline constitutes less than 1%. Analysing corresponding spanloads, lift is found to be distributed unevenly among bottom and top wing, explaining discrepancies found above to some extent. Minor performance benefits are indicated for the crescent biplane configuration in respect to the elliptical system. An elaborate discussion on results based on potential theory is not given here but can be found in Hoefling et al. [12].

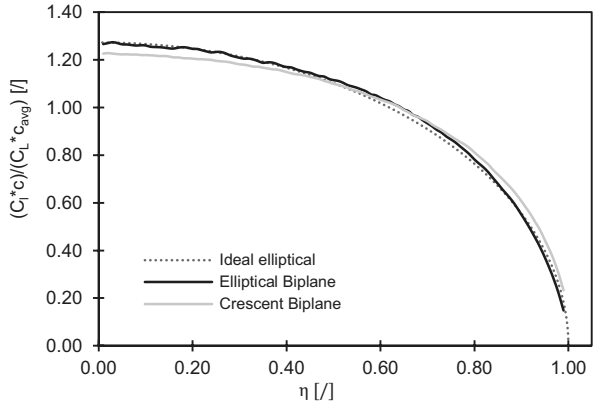

FIG 9. Spanload for elliptical and crescent biplane

Employing standard surface pressure integration technique within *ANSYS Fluent* yields span efficiencies, far below the theoretical baseline and in the range of simple planar wings for both systems. Deviations compared to lifting line theory are of similar magnitude (about 30%) than for the reference systems considered in section 4.1. Results obtained using this technique are therefore not assumed to be plausible. However it should be noted, that this judgment cannot be made based on relative error in respect to biplane theory exclusively, but is founded by experience from other sides and findings in section 4.1 for planar systems.

Span efficiencies delivered by means of farfield analysis are in close consistency with estimates issued by linear potential methodology with a relative deviation of about 1% overall compared to lifting line/biplane theory. Near elliptical shape of associated spanloads depicted in FIG 9 emphasize this result. In contrast to the planar reference systems, the elliptical biplane adopts a more elliptic loading, conflicting with reason given before to vindicate performance benefits of crescent planform. This further contradicts similar findings issued by Hoefling et al [12] using high-order panel method. In this respect, other reasons need to be given to provide meaningful enlightenment of this result.

Analysing spanloads for each lifting surface individually, bottom wing is revealed to produce considerably more lift than the top wing for both highly non-planar systems (compare FIG 10 and FIG 11). Lift created by top wing is accordingly offset from ideal elliptical distribution towards smaller values. Although this appears reasonable, as channel flow in gap between both surfaces induces overspeeds, it does not hold as a valid explanation for prevailing efficiency differences between both systems solely. Moreover, reflecting Prandtl's [23] condition of minimum induced drag of highly non-planar systems, span efficiency of crescent biplane ought to be reduced compared to elliptical biplane as its spanload exhibits lager deviation from the elliptical baseline.

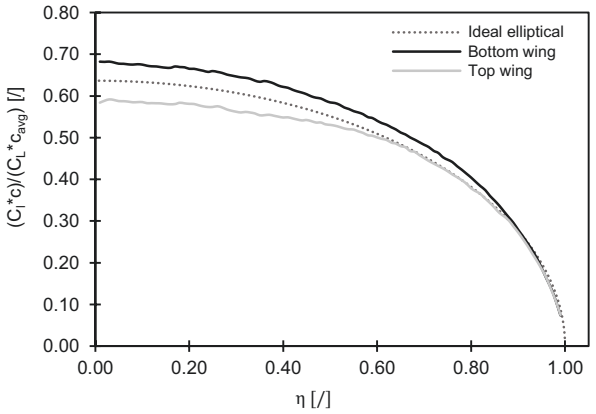

FIG 10. Spanload for elliptical biplane

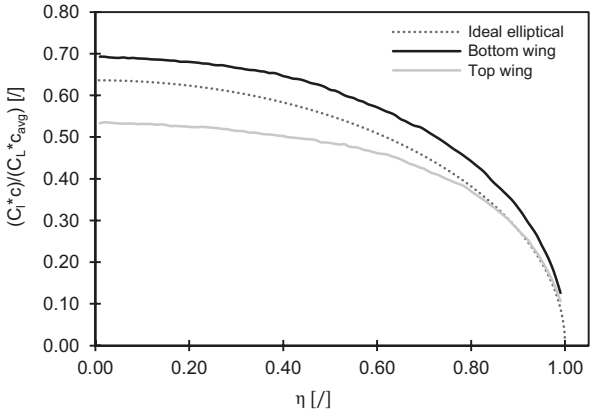

FIG 11. Spanload for crescent biplane

Consulting in addition local downwash distribution given in FIG 12, a consisting explanation can finally be provided. Evidently, crescent biplane produces a more constant downwash pattern than the elliptical biplane at a substantially lower velocity level. While downwash magnitude of elliptical biplane is similar to those given by lifting line theory, downwash of crescent biplane is offset to larger values. This is even more interesting when considering that crescent biplane produces slightly more lift under present flow conditions. Employing equation (12) as an approximate correlation between induced drag per unit span, sectional lift coefficient and downwash velocity, the

present result becomes more acceptable. In other words, although spanload for the crescent biplane shows larger deviations from the ideal elliptical reference, reduced downwash velocities (over)compensate this effect and lead to increased span efficiency in respect to elliptical biplane.

(12) $$C_{di} = -C_l \arctan\left(\frac{w}{V_\infty}\right)$$

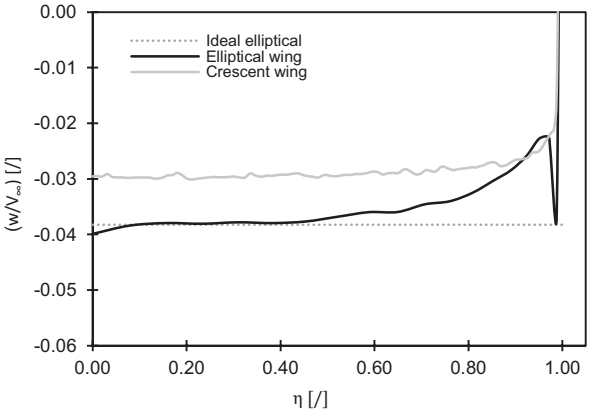

FIG 12. Downwash for elliptical and crescent biplane

Distribution of the latter further experiences a strong downwash peak close to the wing tip, which is assumed to be related to tip vortex roll-up close to the system.

6 CONCLUSION

Implemented Euler based farfield analysis has successfully proven to be a reliably technique to accurately estimate induced drag. Computed span efficiencies for highly non-planar lifting systems investigated are in close consistency with those predicted by linear vortex-lattice methodology. This implies, that the impact of non-linear flow field properties on the induced drag characteristics of present highly non-planar lifting systems are small and can be neglected. Non-planarity of system can therefore not be assumed to introduce or even exaggerate non-linear flow effects on induced drag necessarily. However is must be admitted that configurations studied present a special case within non-planar systems. More complex wing arrangements, deviating from the elliptical chord distribution, may introduce more pronounced effects. This is also supposed for configurations introducing induced lift by vertical geometry components or closed systems like the box wing.

Moreover it could be shown, that spanwise loadings departing from the ideal elliptical distribution are not compelled to introduce major performance deficits for highly non-planar lifting systems. In that context, downwash pattern of the crescent biplane is revealed to be reduced compared to lifting line theory, compensating potential performance deficits experienced by uneven lift distribution. Source of this deviation needs to be studied more in detail, however may be ascribed to higher order effects as these have not be resolved by *AVL*.

Gained results encourage to pursuit implementation of Euler based farfield analysis into conceptual design studies, despite the fact of increased computational effort compared to linear potential methodology (e.g. vortex-lattice method). Discrepancies in spanloads and downwash distribution, not resolved by vortex-lattice approach become important not only within optimization procedures but also considering imposed trim constraints for example.

Additional research effort is required to give more adequate answer to the question of contribution of non-linear flow field properties on the induced drag characteristics of highly non-planar lifting systems in general. This involves detailed studies on prevailing mechanisms of influence as well as analysis of lifting systems with increased complexity.

7 REFERENCES

[1] ANSYS, I. *ANSYS Workbench*.

[2] Bourdin, P. 2002. Planform Effects on Lift-Induced Drag. In *20th AIAA Applied Aerodynamics Conference,* 24-26 June, St. Louis, Missouri, USA. AIAA 2002-3151, doi: 10.2514/6.2002-3151.

[3] Chao, D. and van Dam, C. P. 2004. Wing Drag Prediction and Decomposition. In *22nd AIAA Applied Aerodynamics Conference and Exhibit,* 16 - 19 August, Providence, Rhode Island, USA. AIAA 2004-5074, doi: 10.2514/6.2004-5074.

[4] Demasi, L. 2007. Investigation on the Conditions of Minimum Induced Drag of Closed Wing Systems and C-Wings. *Journal of Aircraft* 44, 1, 81–99, doi: 10.2514/1.21884.

[5] Destarac, D. 2011. Spurious Far-Field-Boundary Induced Drag in Two-Dimensional Flow Simulations. *Journal of Aircraft* 48, 4, 1444–1455, doi: 10.2514/1.C031331.

[6] Destarac, D. and van der Vooren, J. 2004. Drag/thrust analysis of jet-propelled transonic transport aircraft; Definition of physical drag components. *Aerospace Science and Technology* 8, 6, 545–556, doi: 10.1016/j.ast.2004.03.004.

[7] Drela, M. *AVL*. *Athena Vortex Lattice*. Harold Youngren, Aerocraft, Inc.

[8] Ferziger, J. H. and Perić, M. 2002. *Computational methods for fluid dynamics*. Springer, Berlin, New York.

[9] Foong, K. E. and Djojodihardjo, H. 2012. Conceptual Design and Aerodynamic Study of Joined-Wing Business Jet Aircraft. In *28th Congress of the International Council of Aeronautical Sciences,* 23-28 September, Brisbane, Australia.

[10] Gariépy, M., Trépanier, J.-Y., and Masson, C. 2011. Convergence Criterion for a Far-Field Drag Prediction and Decomposition Method. *AIAA Journal* 49, 12, 2814–2818, doi: 10.2514/1.J050865.

[11] Hicken, J. E. and Zingg, D. W. 2010. Induced-Drag Minimization of Nonplanar Geometries Based on the Euler Equations. *Journal of Aircraft* 48, 11, 2564–2575, doi: 10.2514/1.J050379.

[12] Hoefling, J., Schirra, J. C., Spohr, A., and Schaefer, D. 2013. Induced drag computation with wake model schemes for highly non-planar lifting systems. In *Deutscher Luft- und Raumfahrtkongress 2013,* 10-12 September, Stuttgart, Germany.

[13] Hue, D. and Esquieu, S. 2011. Computational Drag Prediction of the DPW4 Configuration Using the Far-Field Approach. *Journal of Aircraft* 48, 5, 1658–1670, doi: 10.2514/1.C031337.

[14] Hunt, D. L., Cummings, R. M., and Giles, M. B. 1999. Wake Integration for Three-Dimensional Flowfield Computations: Applications. *Journal of Aircraft* 36, 2, 366–373, doi: 10.2514/2.2466.

[15] Jansen, P. W., Perez, R. E., and Martins, J. R. R. A. 2010. Aerostructural Optimization of Nonplanar Lifting Surfaces. *Journal of Aircraft* 47, 5, 1490–1503, doi:

10.2514/1.44727.

[16] Jemitola, P. O. and Fielding, J. P. 2012. Box Wing Aircraft Conceptual Design. In *28th Congress of the International Council of Aeronautical Sciences,* 23-28 September, Brisbane, Australia.

[17] Kroo, I. M. 2000. DRAG DUE TO LIFT: Concepts for Prediction and Reduction. *Annual Review of Fluid Mechanics* 33, 587–617.

[18] Kroo, I. M. 2005. *Nonplanar Wing Concepts for increased Aircraft Efficiency*. VKI Lecture series: Innovative Configurations and Advanced Concepts for Future Civil Transport Aircraft, Pisa.

[19] Lam, F. and Maull, D. J. 1993. Induced drag of a crescent wing planform. *Journal of Aircraft* 30, 5, 594–602, doi: 10.2514/3.46387.

[20] Mamla, P. and Galinski, C. 2009. Basic Induced Drag Study of the Joined-Wing Aircraft. *Journal of Aircraft* 46, 4, 1438–1440, doi: 10.2514/1.42084.

[21] Mortara, K. W. and Maughmer, M. D. 1993. A method for the prediction of induced drag for planar and nonplanar wings. *Journal of Aircraft*, 179–189.

[22] Munk, M. 1924. *The minimum induced drag of aerofoils*. NACA Report 121. NACA.

[23] Prandtl, L. 1924. *Induced Drag of Multiplanes*. NACA Technical Notes TN-182. NACA.

[24] Salam, I. R. and Bil, C. 2012. Methodology for a preliminary Design Study of a Box-Wing Airliner. In *28th Congress of the International Council of Aeronautical Sciences,* 23-28 September, Brisbane, Australia.

[25] Salam, I. R. and Bil, C. 2012. Preliminary Aerodynamic and Structural Design Tradeoff for a Box-Wing Airliner. In *50th AIAA aerospace sciences meeting including the new horizons forum and aerospace exposition 2012,* 9-12 January, Nashville, Tennessee, USA. doi: 10.2514/6.2012-251.

[26] Smith, S. C. 1996. *A Computational and Experimental Study of Nonlinear Aspects of Induced Drag*. NACA Technical Notes TN-3598. NASA.

[27] Smith, S. C. and Kroo, I. M. 1993. Computation of Induced Drag for Elliptical and Crescent-Shaped Wings. *Journal of Aircraft* 30, 4, 446–452.

[28] Smith, S. C. and Kroo, I. M. 1997. Induced Drag Computations on Wings with Accurately Modeled Wakes. *Journal of Aircraft* 34, 2, 253–255, doi: 10.2514/2.7570.

[29] Sun, W.-C., Broichhausen, K., and Seifert, J. 2008. Promissing Future Aircraft Concepts - ESTOL. In *26th Congress of the International Council of Aeronautical Sciences,* 14-19 September, Anchorage, Alaska, USA.

[30] van Dam, C. P. Induced-drag characteristics of crescent-moon-shaped wings. *Journal of Aircraft* 24, 2, 115–119, doi: 10.2514/3.45427.

[31] van Dam, C. P. and Nikfetrat, K. 1992. Accurate prediction of drag using Euler methods. *Journal of Aircraft* 29, 3, 516–519, doi: 10.2514/3.46194.

[32] Verstraeten, J. G. and Slingerland, R. 2009. Drag Characteristics for Optimally Span-Loaded Planar, Winglетted, and C Wings. *Journal of Aircraft* 46, 3, 962–971, doi: 10.2514/1.39426.

[33] Vos, J. B., Sanchi, S., and Gehri, A. 2010. DPW4 Results Using Different Grids Including Near-Field/Far-Field Drag Analysis. In *28th AIAA Applied Aerodynamics Conference,* 28 June - 1 July, Chicago, Illinois, USA.